1991-05-15

Medium- to large-scale atmospheric variability during the Frontal Air-Sea Interaction Experiment

Davidson, K. L.; Boyle, P. J.; Gautier, C.; Hanson, H. P.; Khalsa, S. J. S.

American Geophysical Union

Journal of Geophysical Research, Vol. 96, no. C5, pp. 8531-8551, May 15, 1991
https://hdl.handle.net/10945/46803

JOURNAL OF GEOPHYSICAL RESEARCH, VOL. 96, NO. C5, PAGES 8531–8551, MAY 15, 1991

Medium- to Large-Scale Atmospheric Variability During the Frontal Air-Sea Interaction Experiment

K. L. DAVIDSON AND P. J. BOYLE

Department of Meteorology, Naval Postgraduate School, Monterey, California

C. GAUTIER

Department of Geography, University of California, Santa Barbara

H. P. HANSON AND S. J. S. KHALSA

Cooperative Institute for Research in Environmental Sciences, Boulder, Colorado

Shipboard, aircraft, and satellite atmospheric data are examined to determine the representativeness of the Frontal Air-Sea Interaction Experiment (FASINEX) intensive measurement period, Phase II, in terms of climatology, atmospheric forcing, the general structure of the marine atmospheric boundary layer (MABL), and variability in boundary layer properties affecting air-ocean dynamics and thermodynamics. With regard to climatology, conditions observed during the intensive period were typical in terms of air-sea temperature differences, surface pressure patterns, cloud cover, and storm tracks. Storm system variabilities, such as the air temperature behind cold fronts, wind stress maxima occurring after frontal passage, the times for clockwise vector wind shifts associated with the frontal systems, and the systems' speeds, are estimated and emphasized in synoptic-scale characterizations, since these can be related to observed ocean responses. The local ocean surface variability was observed to have an influence on regional boundary layer properties and on air-sea interaction parameters even in the presence of the atmospheric storms.

1. BACKGROUND

Transfers of heat, moisture, and momentum between the atmosphere and ocean on scales of 10–100 km play an important role in air-ocean dynamics and thermodynamics in the Frontal Air Sea Interaction Experiment (FASINEX) region. FASINEX took place in the mid-latitudes, off the east coast of the United States, (26°–28°N, 69°–71°W) during the winter and spring of 1986. It was designed to increase understandings of air-ocean interactions in the presence of a sea surface temperature (SST) front [*Weller*, this issue]. We will examine medium- to large-scale atmospheric conditions during the intensive measurement period, Phase II, that took place from January through early March of 1986.

The FASINEX region is characterized by a pattern of atmospheric frontal systems traveling through the area along eastward tracks associated with northeastward propagating cyclones that were centered north of the region. Atmospheric forcing is greatest at this location in the vicinity of storms, and the frequency, speed, path, and intensity of storm systems passing over the area determine the magnitude of the effects of this forcing on the oceanic boundary layer (OBL). Conversely, ocean surface influence on the atmosphere during FASINEX can be seen most easily in the periods between the passage of atmospheric frontal systems, in the absence of strong advective forcing.

Medium- to large-scale ocean dynamic features not necessarily associated with the SST front were also studied in FASINEX investigations. Such ocean responses to atmospheric forcing during FASINEX are presented by *Weller et al.* [this issue], hereafter referred to as Weller et al. Explanations of the role of the atmospheric forcing on observed medium- to large-scale ocean responses require knowledge of spatial as well as temporal variations of the forcing. Moored array results on the oceanic near-inertial oscillations indicate the important role of the clockwise-rotating component of the wind stress. The tracks of storms, the associated vector stress variations, and their time scale variations determined the resonant atmospheric energy that excited the observed near-inertial and clockwise-rotating oscillations in the ocean. It will be shown that the tracks of the atmospheric systems and the time scales of the vector wind changes associated with them would lead to resonant forcing of near-inertial oscillations.

The curl of the wind stress determines the "pumping" of the ocean interior and depends on the spatial scale of the storm systems and the stress amplitude variations across these systems. It was not possible to compute the curl of the stress from the ship data, but the variation of the ship-obtained stress values across the cyclones will be presented.

Based on ocean responses, Weller et al. estimated 700 km as the representative scale of the passing atmospheric systems. This scale will be shown to be within the range of scales determined from time series of meteorological parameters obtained at the ships and buoys. Weller et al. also observed that it took 5–10 days for the ocean fronts to pass through the buoy array.

The primary purpose of this paper is to present information on spatial and temporal variations of the FASINEX mesoscale and synoptic-scale atmospheric conditions relevant to observed ocean response and to provide a framework

Paper number 91JC00435.
0148-0227/91/91JC-00435$05.00

for considering the observed forcing of the atmosphere by the ocean surface described elsewhere [*Friehe et al.*, this issue]. Using climatology as a background, the atmospheric features mentioned above will be described with a view toward characterizing the unique features of the FASINEX area.

2. Climatological Perspective

To interpret the conditions during FASINEX more accurately and to determine the representativeness of the results, it is necessary to consider the climatology of the region. One should know, in the context of climatology, whether the number of storms during the experiment was typical. How did the mesoscale sea surface temperatures, surface winds, and high-pressure ridge commonly found in this area compare to the climatological mean? These are important considerations when applying the results of FASINEX studies.

The large-scale climatology of the area is discussed by *Hanson et al.* [this issue]. Here we will concentrate on the intensive measurement period, January through March 1986, and will compare monthly means of several variables measured during FASINEX with climatological means for those variables, to get an idea of the deviation of the FASINEX intensive measurement period from the norm. Figures 1 and 2 present these comparisons; climatology is given in the left column, FASINEX monthly means are on the right. The FASINEX measurement area is represented by the triangle. Data for Figures 1 and 2 were extracted from the Comprehensive Ocean-Atmosphere Data Set (COADS); a description of COADS is given by *Woodruff et al.* [1987].

In Figure 1 the climatological surface pressure fields and wind vectors show the expected westerly flow in the mid-latitudes and easterly flow in the subtropics. The beginning of the formation of the summertime subtropical high, with the ridge building from the east, is particularly evident in March (bottom panel). The monthly mean for 1986, by comparison, exhibits a more complicated pressure pattern, as one would expect from the shorter averaging period. The general location of the mid-latitude storm systems north of the measurement area is reflected in the pressure pattern of Figure 1. The fronts associated with the storms passed through the FASINEX region, but the centers of the associated low-pressure systems passed to the north of the area. This is as expected from climatology; climatological patterns are displayed in the atlas by *Whittaker and Horn* [1982]. This track leads to clockwise changes in wind direction at a point in the FASINEX area, as low-pressure systems (with counterclockwise-rotating winds) and high-pressure systems (with clockwise-rotating winds) pass to the north of the ships and buoys.

The atmospheric forcing due to the storms can be considered fairly representative of the region. The high-pressure ridge, centered about 27°N, was somewhat stronger in January and March than would be expected from climatology, with a tendency for southerly winds at the array, but the trough over eastern North America was only slightly deeper than normal [*Barston*, 1987]. The storms may have been slowed down somewhat by the blocking ridge. The storm frequency of one system every 3–5 days is normal for the area, according to climatology [*Whittaker and Horn*, 1982].

In terms of sea surface temperature variations, sea-air temperature differences, and total cloud cover, conditions during January–March 1986 were also roughly what one would expect from climatology. Monthly averages for March, chosen as a representative month, appear in Figure 2, compared with COADS-derived climatology. The SST pattern shows temperatures about 0.5°C warmer than normal at the FASINEX site; the sea-air temperature differences are also about as expected, with a value of 1.5°C. The total cloud cover is given in tenths in the bottom panel of Figure 2. In the FASINEX area, the average cloud cover is around 55%. The dominant feature is the maximum to the north of the triangle, representing the increased cloud cover associated with storm systems.

These large-scale views of the meteorological conditions in the western North Atlantic provide a framework for considering the individual storms that passed through the FASINEX area and the characteristics of the atmosphere in between storms. The conditions to be considered here occurred when the R/V *Oceanus* and R/V *Endeavor* were collecting data in the vicinity of the moored array. During this time several research aircraft were also operating in the region. Data from the NOAA P-3 and NCAR Electra will be presented in this paper.

3. Relation of Sea Surface Temperature Gradient to Cloudiness

Cloudiness was analyzed using the visible and infrared measurements made from both polar-orbiting (NOAA series) and geostationary satellites (GOES series). During the investigation, two advanced very high resolution radiometer (AVHRR) observations were obtained per day from the NOAA 9 satellite, and half-hourly visible-infrared spin-scan radiometer (VISSR) observations were acquired from the GOES 6 satellite. Although satellite observations do not offer a three-dimensional view of clouds, they do provide spatial information of cloud signatures at different sensor observing wavelengths.

Satellite data was validated using information collected from the moored buoys and both the R/V *Endeavor* and R/V *Oceanus*. The full methodology of the validation is described by *Bates and Gautier* [1989]. An estimate of the effect of the clouds on the surface solar irradiance is given by the equivalent cloud parameter (*CL*). It is computed as one (1) minus the ratio of the satellite-estimated solar irradiance to a simulated irradiance for a corresponding clear sky. The analysis showed, as expected, periods several days in length of relatively clear conditions with minimal cloud effects (for example, February 5–9, in Figure 3*a*) alternating with periods of comparable length of low surface irradiance with strong cloud effects (for example, February 25 to March 1, shown in Figure 3*b*). These low values of surface solar irradiance were often associated with frontal passages. As is well known, broad multilayered clouds usually form in the strong baroclinic zones of mid-latitude cyclones and thicken as the cyclone intensifies. The clouds usually bulge toward the cold air and reduce the surface solar irradiance by reflecting and absorbing solar radiation because they contain large amounts of liquid water.

The monthly mean cloud effects, illustrated in Figure 4 for the period February 5 through March 6, indicated a relatively smooth meridional gradient (from 0.37 in the north to 0.23 in the south), slightly perturbed by a weak zonal gradient (0.02 per 2° longitude) centered around 70°W. The satellite analysis thus suggests a minimal local effect of the thermal front on the mean cloudiness.

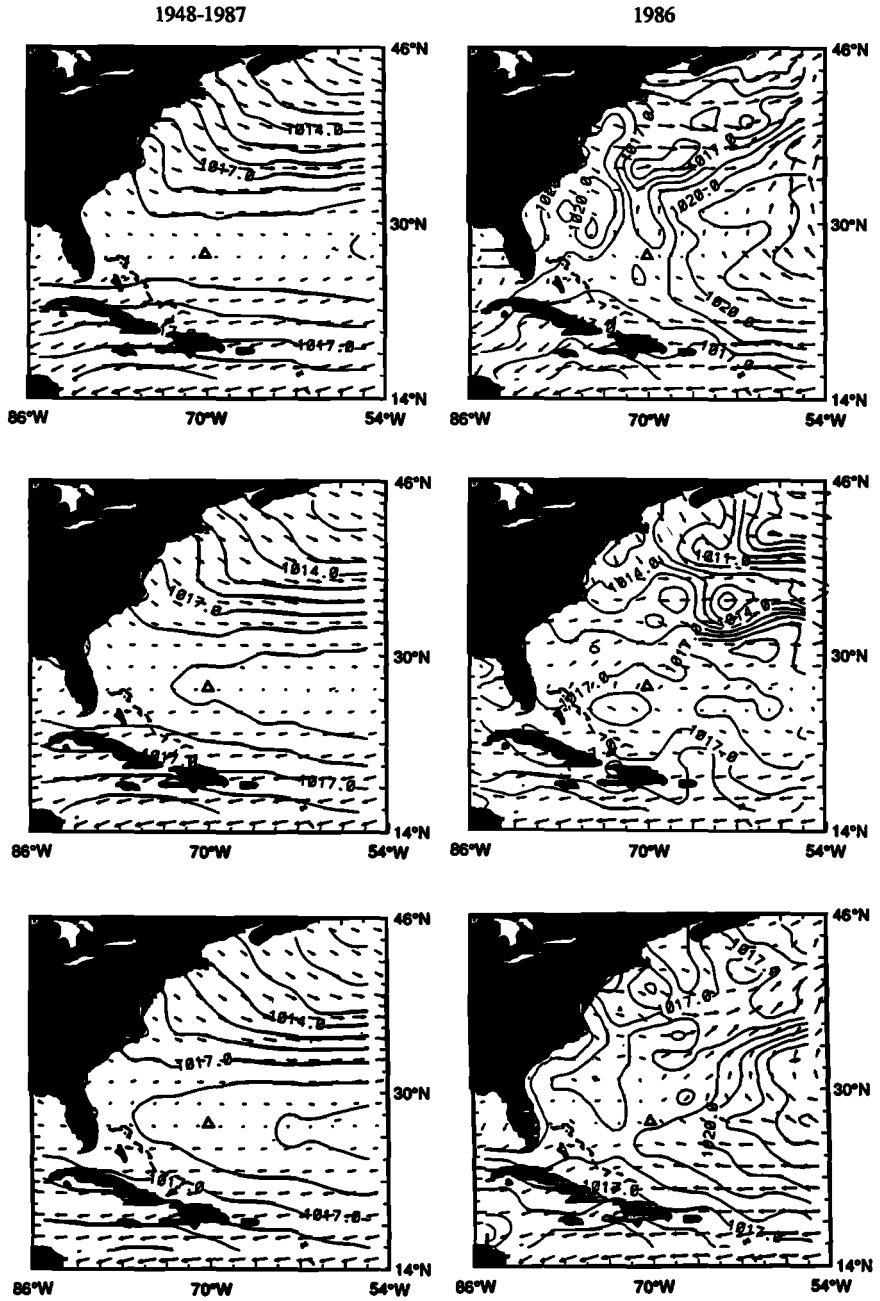

Fig. 1. Surface pressure (in millibars) and wind vectors from COADS. (Left) The long-term average and (right) conditions during 1986 for (top to bottom) January, February, and March. The distance between tick marks represents a 10 m s^{-1} wind vector, derived from the averaged zonal and meridional wind components. The triangle shows the position of the FASINEX moored array.

4. Regional Atmospheric Surface Layer Variation in Vicinity of SST Front

National Meteorological Center (NMC) sea level, operational pressure analyses provide a general idea of atmospheric cyclone and associated frontal system movements that affected the FASINEX area. However, since they are an operational product and depend heavily on satellite data and the availability of surface data over the sea, they do not provide the detail of shipboard observations on the progress of cyclones within the FASINEX area.

Measurements of sea and air temperature, moisture, pressure, relative wind, and turbulent kinetic energy dissipation were made from both the R/V *Endeavor* and R/V *Oceanus* from February 14 through March 7, 1986. Rawinsonde launches were also made from both ships. Time series in Figure 5 are of sea level pressure, humidity, wind speed and direction, air and sea temperatures, turbulent heat flux (sensible, latent, and total), surface wind stress, and surface layer stability (z/L) as made from R/V *Oceanus*. The same time series, as measured from R/V *Endeavor* are given in Figure 6.

Wind stress results in Figures 5*e* and 6*e* were derived from high-frequency turbulence intensity measurements utilizing the turbulent kinetic energy inertial-dissipation method de-

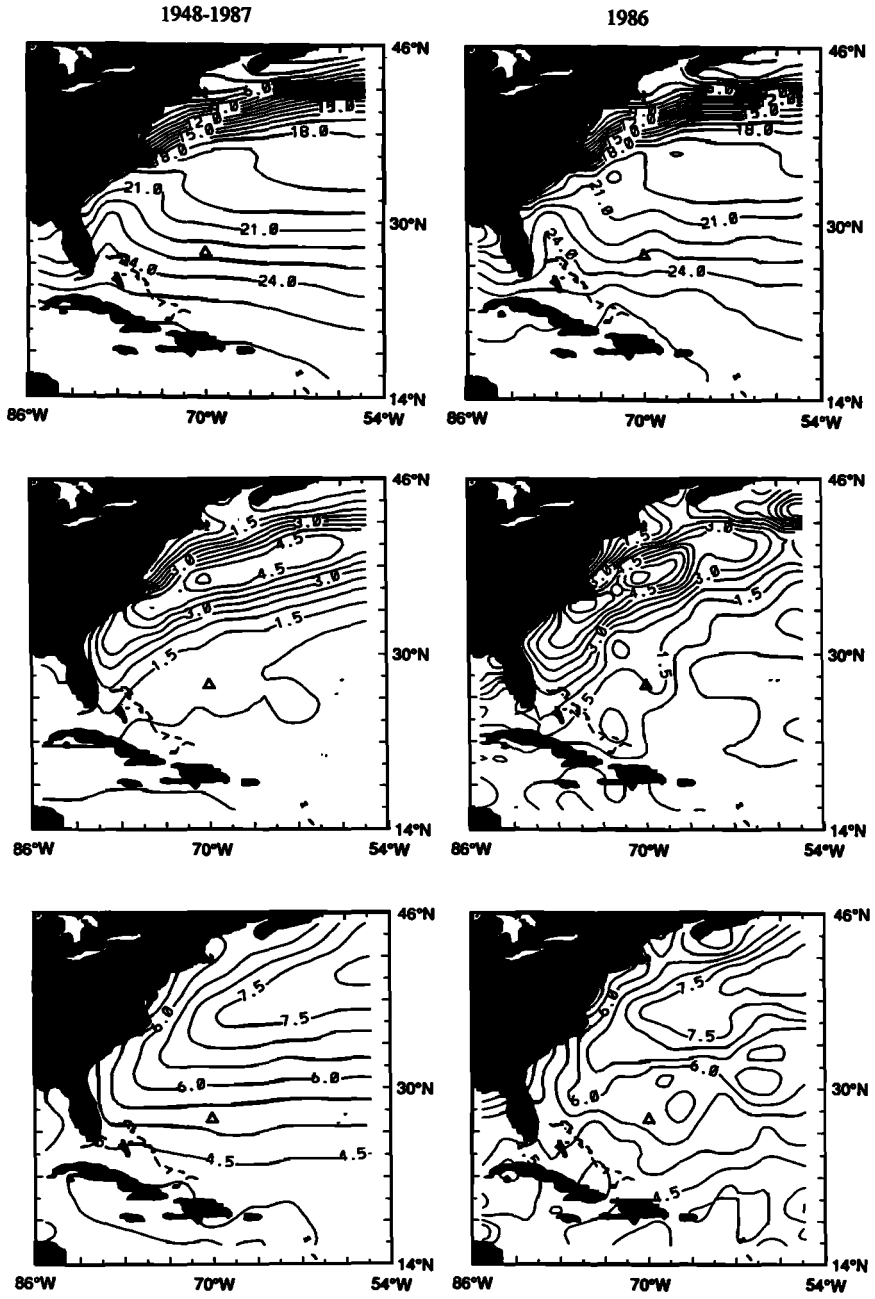

Fig. 2. (Top) March sea surface temperature (in degrees Celsius), (middle) sea-air temperature difference (in degrees Celsius), and (bottom) cloud cover (in tenths) from COADS. (Left) the long-term average and (right) conditions for March 1986. The triangle shows the position of the FASINEX moored array.

scribed by *Fairall et al.* [1990], shown by individual points (crosses), and from the mean wind, temperature, and humidity measurements using *Smith*'s [1988] wind- and stability-dependent drag coefficient formulation, shown by the solid curve. The inertial-dissipation method wind stress and drag coefficient derived values are from 20- and 30-min averages for R/V *Endeavor* and R/V *Oceanus*, respectively. The latter are shown because Weller et al. based their forcing interpretations on bulk-derived wind stress values using the buoy data. We believe knowledge of differences between the two estimates during maximum forcing will be useful in considering their results. The drag coefficient formulation used by Weller et al. [*Large and Pond*, 1981] is 10% higher than that used by *Smith* [1988] for these values in the maximum stress ranges. This difference is not considered to be a factor in descriptions presented here.

Actual procedures used in these inertial-dissipation stress derivations are described by *Skupniewicz and Davidson* [1991] and are very similar to those presented by *Fairall et al.* [1990]. An error analysis of similarly obtained shipboard inertial-dissipation wind stress values by K. L. Davidson, R. G. Onstott, J. A. Johannessen, P. J. Boyle, R. H. Shuchman, O. Skagseth, and C. E. Skupniewicz (Wind stress and radar backscatter observations of ocean surface properties from a ship in NORCSEX, submitted to the *Journal of Geophysical Research*, 1991) yielded a 15%

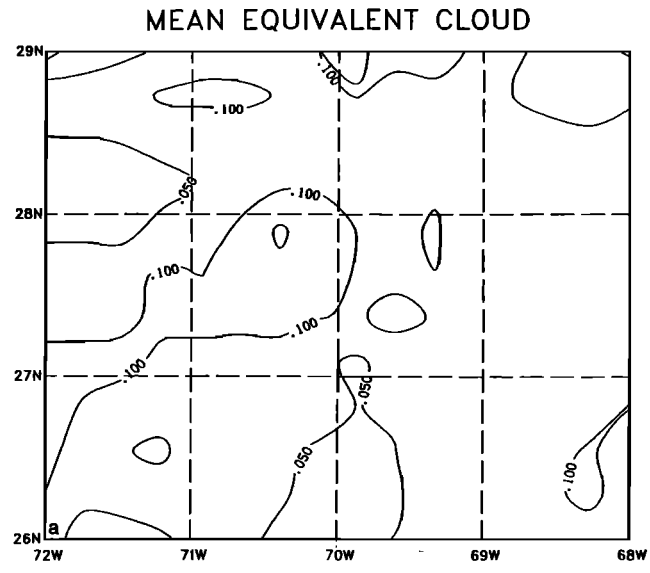

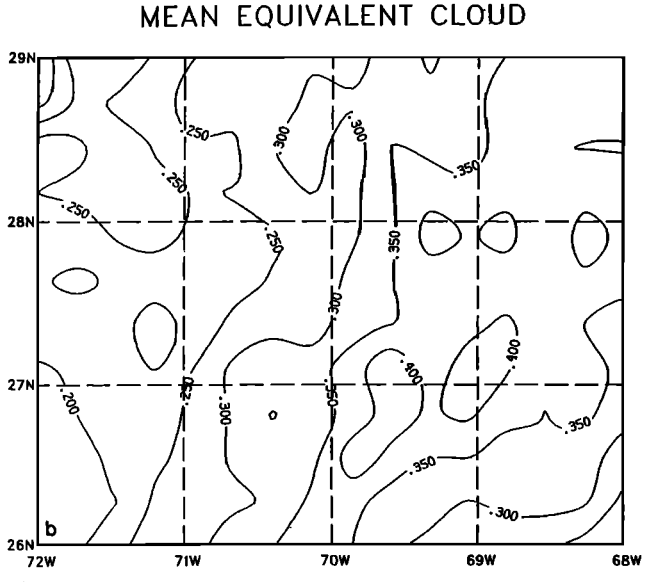

Fig. 3. Mean equivalent cloud parameter (*CL*) (see text for definition) for (*a*) February 5–9 (*b*) February 25 to March 1.

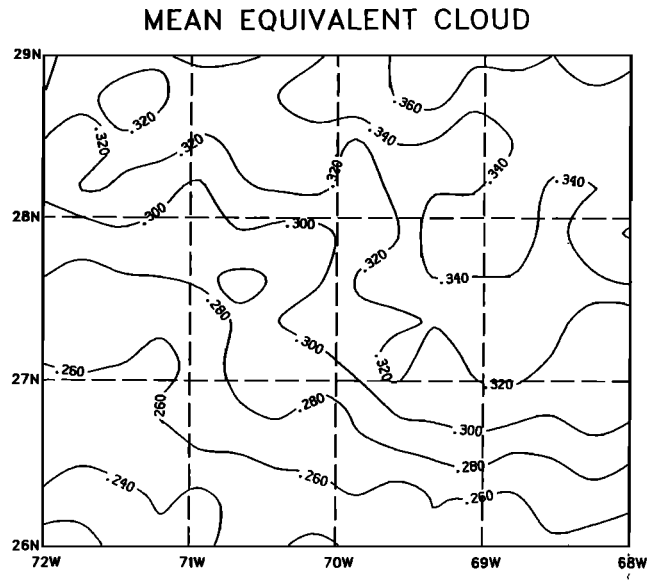

Fig. 4. Thirty-day averaged mean equivalent cloud parameter (*CL*) for period February 5 to March 6.

random error for near-neutral stratifications and an estimated 25% error for stable stratifications encountered with these data.

Turbulent heat fluxes in panel D of Figures 5 and 6 were derived from mean wind, temperature, and humidity values using the formulation of *Smith* [1988]. Calculations of the heat fluxes were also made using the inertial-dissipation derived u_*, and they were larger than the bulk-derived values during periods when inertial-dissipation u_* values were larger than the bulk values.

Evident in Figures 5 and 6 are the continual and often rapid changes in atmospheric synoptic-scale forcing conditions during FASINEX Phase II. The frequent frontal passages are clearly evident in the bulk meteorological variables as well as in the surface layer stress. Seven frontal passages occurred when the ships were collecting data. Frontal passages are indicated by arrows between Figures 5*a* and 6*a* and Figures 5*b* and 6*b*. An examination of the identified frontal passages shows that they generally occurred at 3- to 5-day intervals, except for the fronts on February 13 and 15 that were separated by less than 48 hours and a pair of fronts on February 25 that were separated by less than 10 hours. In the following discussions the periods of vector wind and air temperature and humidity variability associated with these storm fronts will be referenced by the day of the cold front passage. The "frontal passage" days are February 13, 15, 20, and 25 and March 1 and 5 and correspond to "low days" of February 14, 16, 21, and 26 and March 1 and 5 referenced by Weller et al.

Figures 5 and 6 also provide a continuous record of in situ measurements of conditions between storm systems, when small-scale circulations in the atmosphere are most likely to be affected by the SST front. As will be illustrated, however, the influence of a cold front may be important up to a day and a half after the front has passed, complicating the picture of air-ocean dynamics over the 3–5 days between frontal passages.

During the periods when high-pressure systems dominated the area, air temperature varied only slowly, ranging from approximately 18° to 24°C, changing roughly 2°C over time periods of 36 hours. Wind speeds during these undisturbed periods were generally below 8 m s^{-1}. Frontal systems brought increased wind speeds, with a maximum of about 20 m s^{-1}, clockwise changes in wind direction, and air temperature drops of up to 6°C, with the passage of the cold front. Total turbulent heat flux values approaching 700 W m^{-2} occurred over 12- to 18-hour periods, and wind stress values above 0.6 N m^{-2} occurred with storm wind maxima.

The relation of the wind direction to the SST front affects the dynamics of the local air-sea interaction, determining the characteristics of the marine atmospheric boundary layer (MABL), as will be discussed in section 6. *Eriksen et al.* [this issue] describe the nature and variability of the oceanic frontal locations. It is evident in Figures 5 and 6 that a large percentage of time the wind direction was either from northerly or southerly directions, blowing roughly perpendicular to the main SST front. This large percentage of

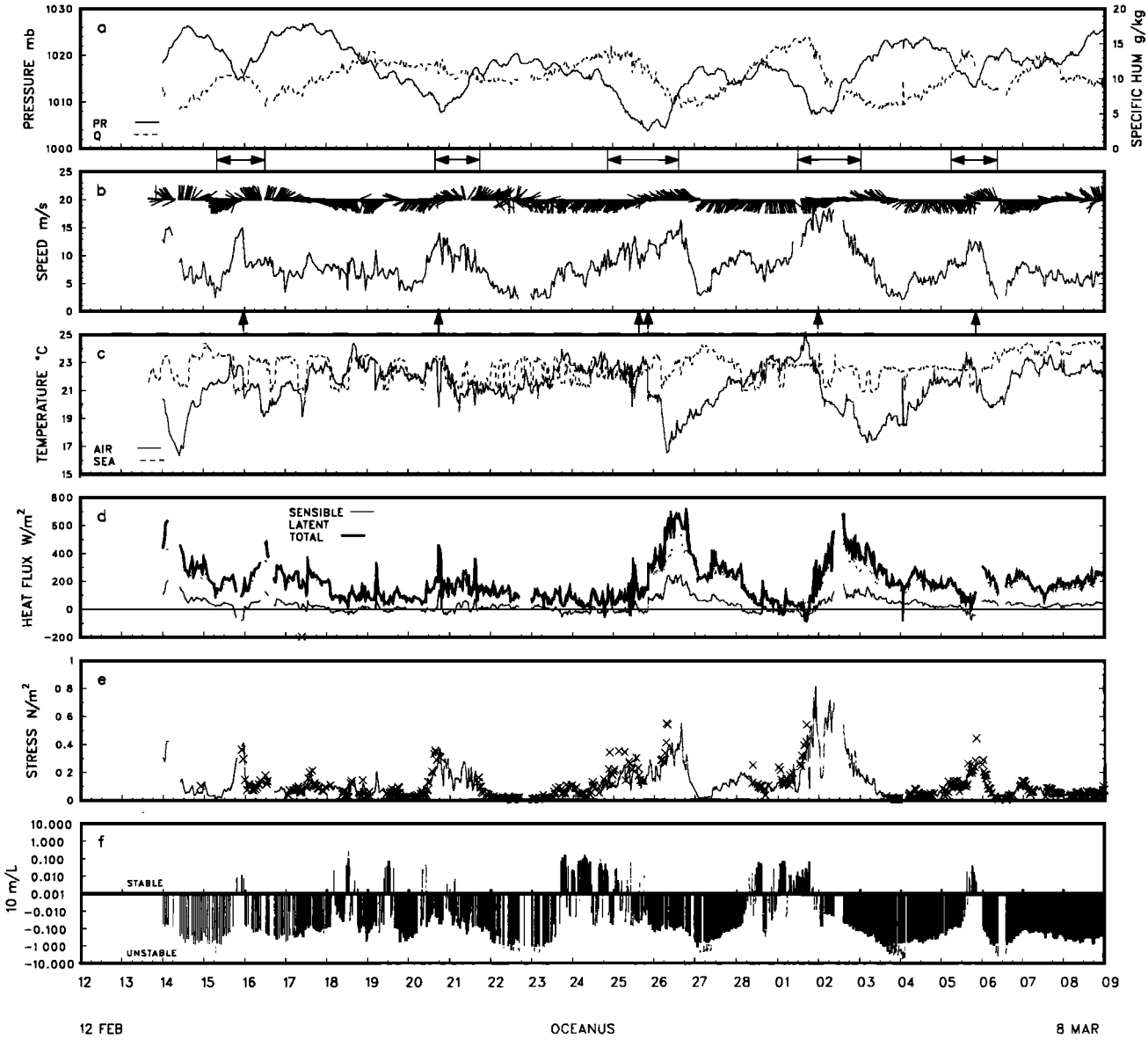

Fig. 5. Surface layer measurements during FASINEX from R/V *Oceanus* of (*a*) Surface pressure and relative humidity (in percent) (dashed curve); (*b*) 10-m wind speed (in meters per second) and wind direction (barbs); (*c*) air (solid curve) and sea surface (dashed curve) temperature (in degrees Celsius); (*d*) heat flux (in watts per square meter), where heavy solid curve is total, light solid curve is sensible, and dashed curve is latent heat flux; (*e*) Surface and wind stress, where individual points (crosses) are inertial-dissipation determined and lines are bulk determined; and (*f*) z/L, where z is 10 m.

cross-front flow occurred because of the almost continuous existence of transiting surface pressure troughs during the period; that is, the stationary subtropical high was not a feature of the period.

5. Influence of Storm Front Systems on Variability of Atmospheric Forcing Parameters

In this section we examine atmospheric variability associated with storm front passages with regard to forcing of the ocean and to the SST front's effect on the overlying atmosphere. In most storm situations the large-scale atmospheric forcing dominated over smaller-scale effects that could have been due to the existence of the SST front. The effects of even a 2°C SST front will be reduced when a storm system brings an air-sea temperature difference greater than 3°C. The signatures of atmospheric forcing variations are similar among storms, but the amplitudes differ. In general, atmospheric conditions in storms masked any effect of the SST front, but this was not true in all cases, the storm system of March 1 being a notable exception, as will be described in section 5.5.

Each storm had its own characteristics with regard to ocean responses, as described by Weller et al. Whereas the time series in Figures 5 and 6 characterize variations at specific locations, the NMC-analyzed surface weather maps in Figure 7 characterize the medium- to large-scale spatial variations. Figures 7*a*–7*f* correspond to storm situations that will be described in the following subsections. The top panel

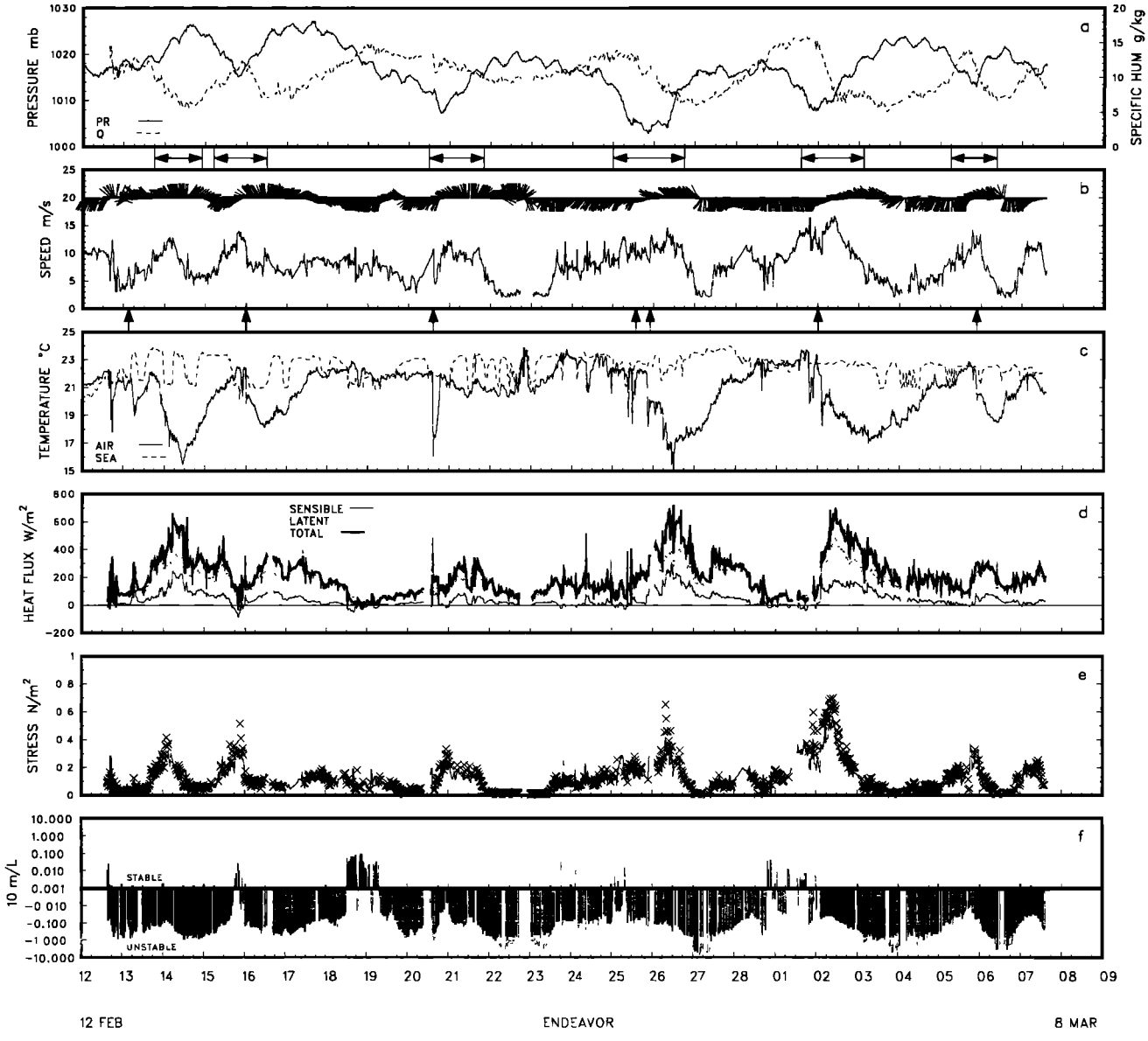

Fig. 6. Same as Figure 5, except for R/V *Endeavor*.

of each of these figures represents a time before a frontal passage, the middle panel a time near the passage, and the bottom panel a time following passage.

Parameters were derived to estimate time and distance scales and the intensity of the atmospheric forcing related to ocean responses and to those used by Weller et al. These were derived from information within the ship as well as the buoy time series and by using the NMC surface weather patterns for guidance. Wind stress and total heat flux maxima observed from either ship and derived values for three storm parameters appear in Table 1.

Storm parameters used by Weller et al. that could be derived from in situ time series were (1) a translation speed of the storm, (2) a spatial scale of the storm, and (3) a time interval corresponding to the period when the system was passing by the ships, during which the vector wind forcing changed in a clockwise direction. The change was generally from a southerly to a northerly direction. We will hereafter refer to this period as the local residence time of the system. In some cases the wind direction shift went through a 180° change, or half cycle, but in other cases it did not go through the entire half cycle, owing to the relation of the location of the ships and buoys to the center of the low-pressure system.

Estimates of the local residence times of the systems were determined from wind direction time series from both ships, with guidance from time series of air temperature, pressure, and wind speed. The lengths of these periods will be compared with the local inertial period of 26.4 hours at the moorings given by Weller et al. The selected local residence times at each ship are indicated above Figures 5*b* and 6*b*. The beginning and ending points of these periods are admittedly subjective, but estimates aid in relating the atmospheric variability to observed ocean variability.

The storm translation speeds were necessary to estimate the spatial scale of the systems as well as to further determine the storms' characteristics. It is recognized that the frontal translation speeds are not necessarily the same as the translation speeds of the storm wind maxima. However, we

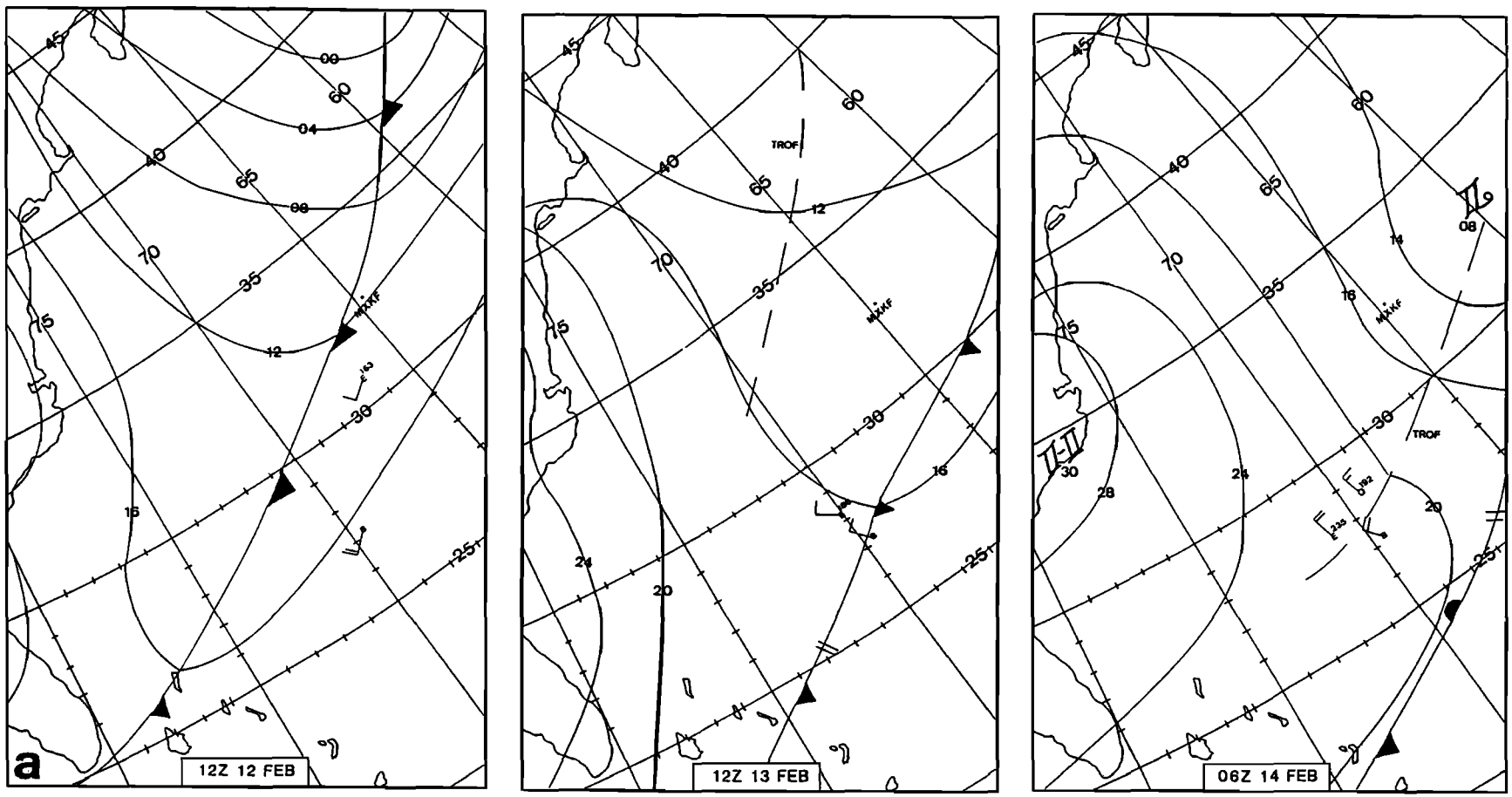

Fig. 7. NMC surface pressure and frontal maps (1200 UT, except February 20, which is 0600 UT) with positions of R/V *Oceanus* and R/V *Endeavor* indicated by labeled wind barbs. (*a*) February 12–14, (*b*) February 14–16, (*c*) February 19–21, (*d*) February 24–26, (*e*) March 1–3, and (*f*) March 4–6.

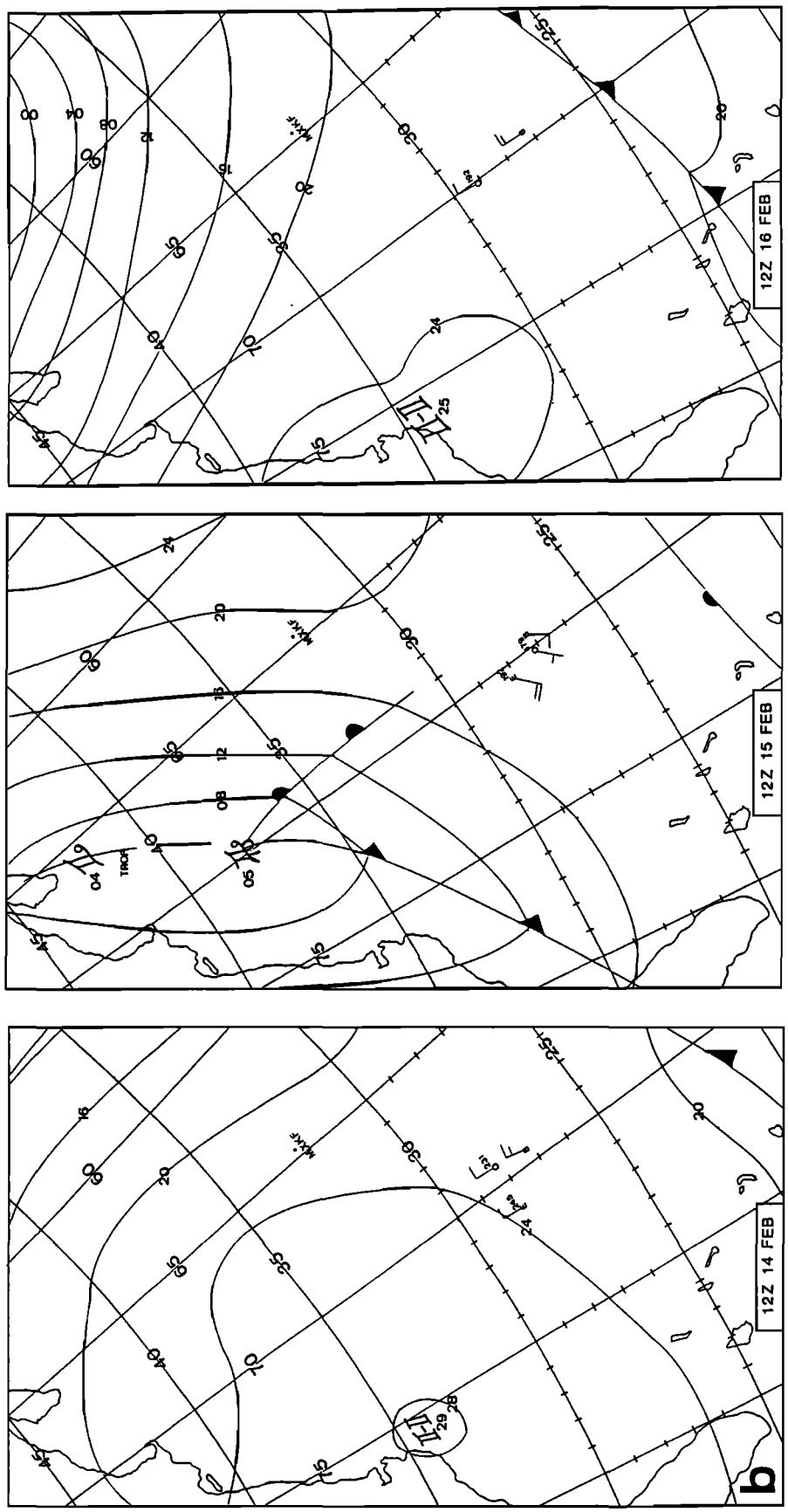

Fig. 7. (continued)

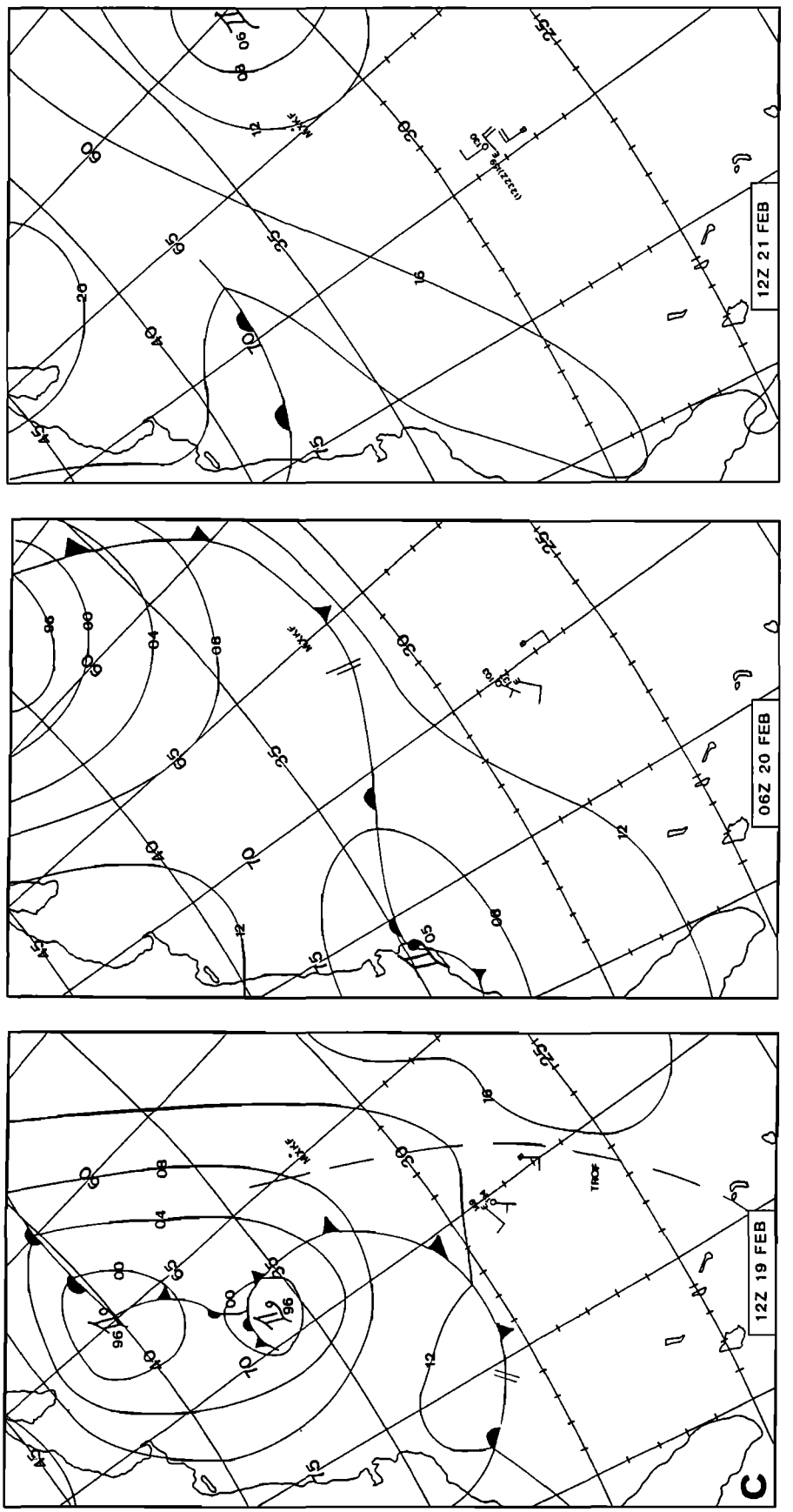

Fig. 7. (continued)

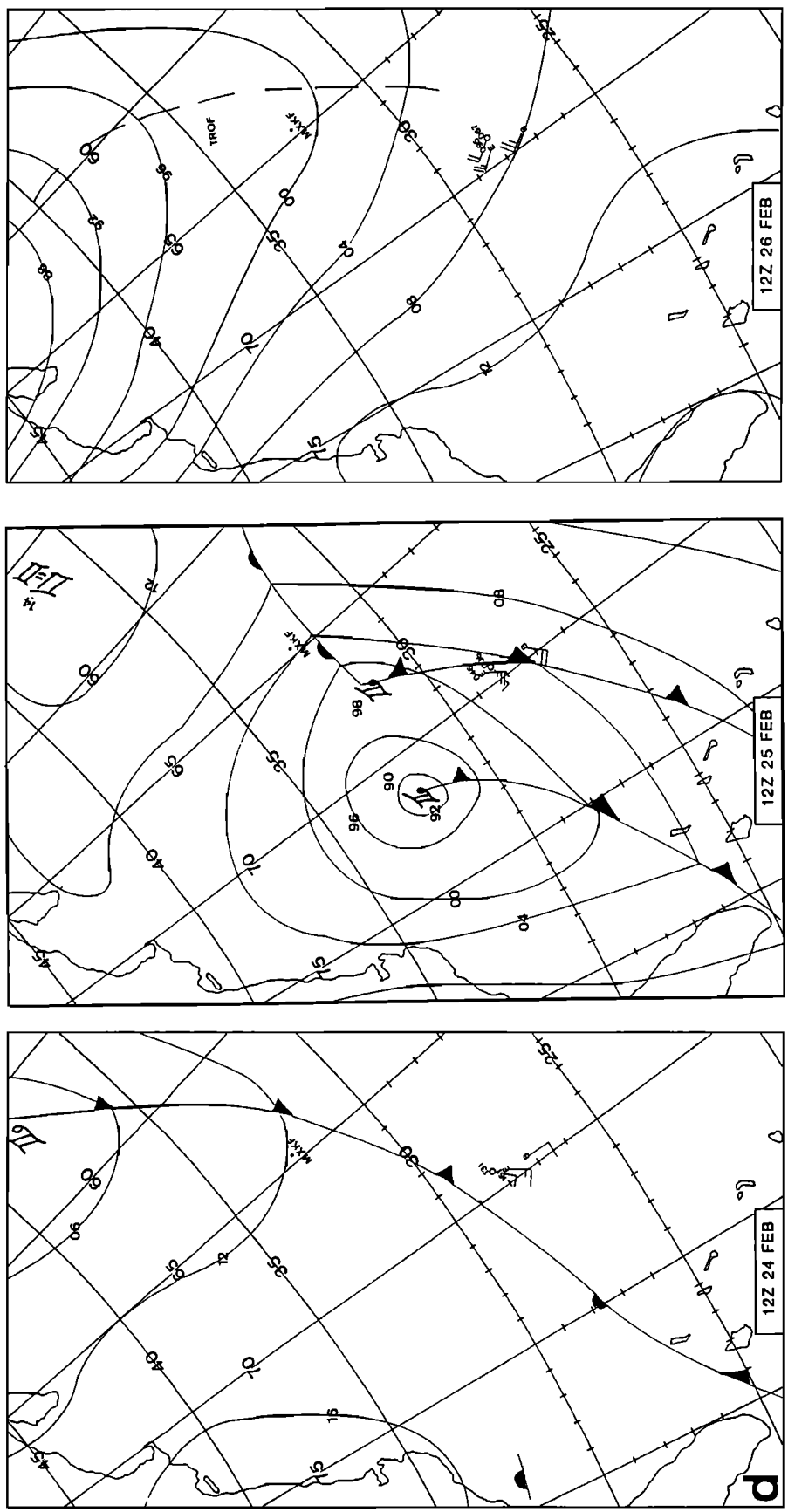

Fig. 7. (continued)

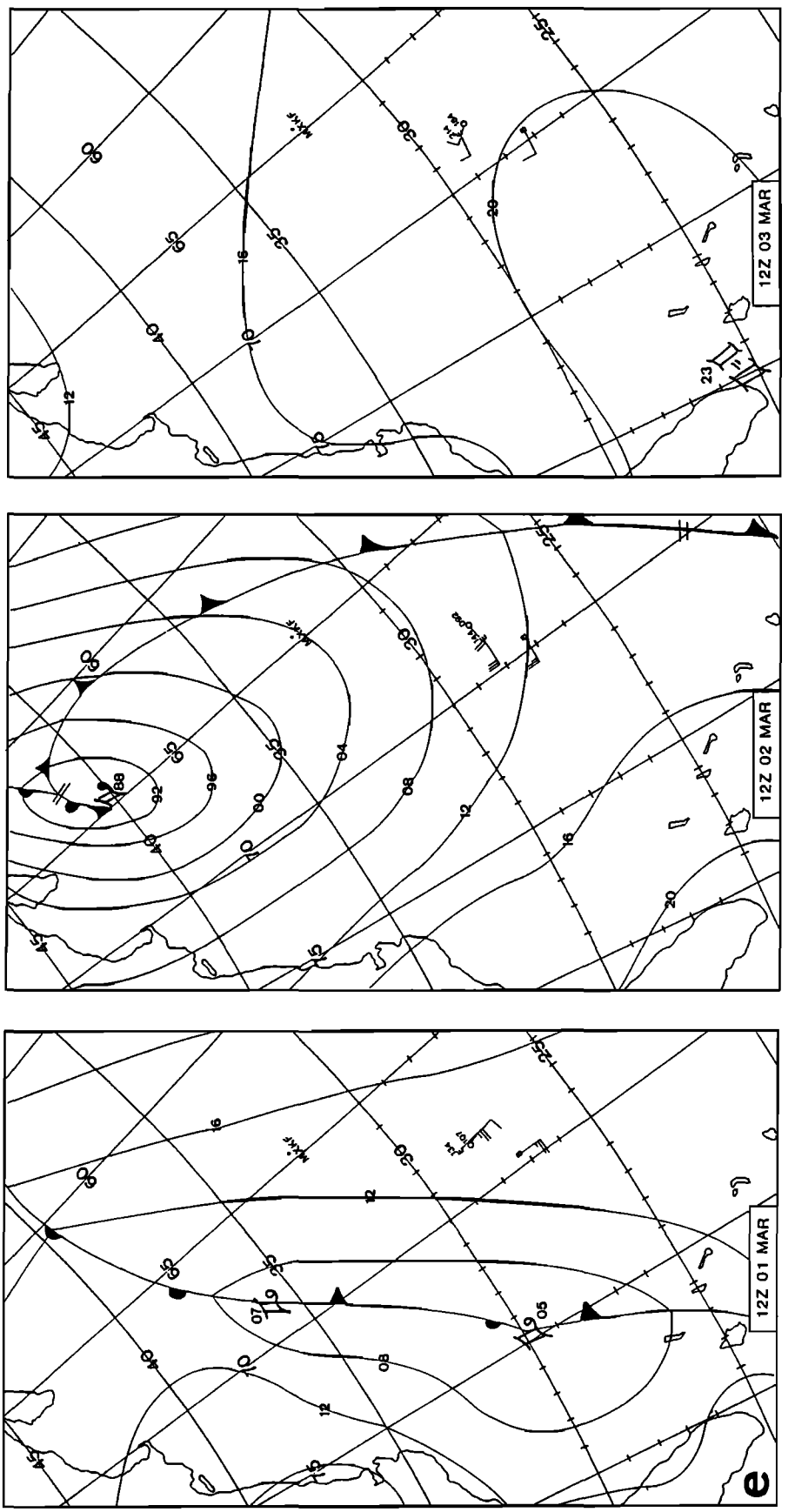

Fig. 7. (continued)

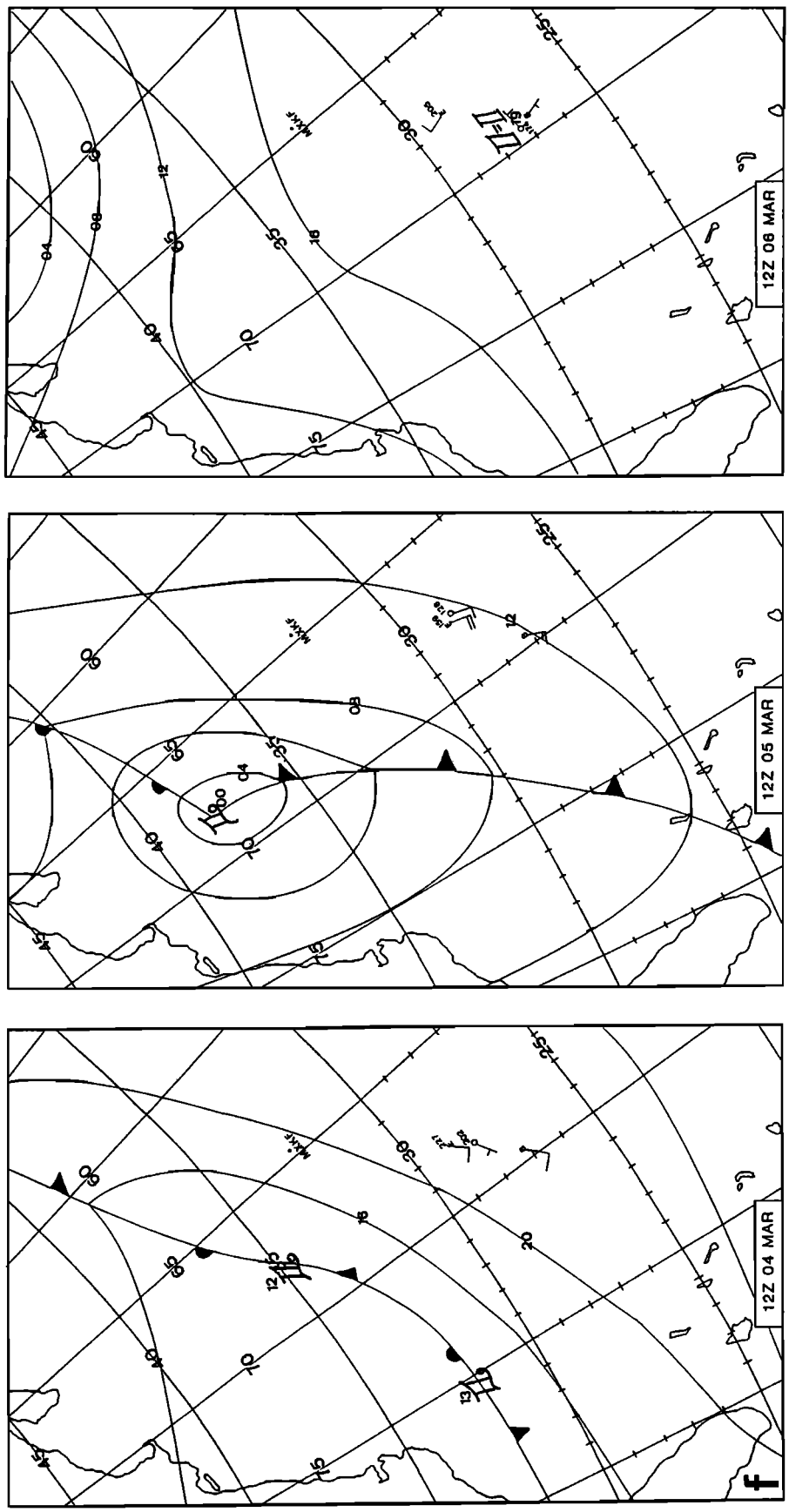

Fig. 7. (continued)

TABLE 1. Low-Pressure System Parameters

Storm System	Date	Storm Parameters: Residence Times Ship	Hours	Average	Translation Speed, km h^{-1}	Spatial Scale, km	Maximum Fluxes: Stress, N m^{-2}	Ratio	Total Heat, W m^{-2}
1	Feb. 13	END	26	26*	27†	702‡	0.40§	1.50	631
2	Feb. 15	END	31	30	27	810	0.50	1.75	479
		OCE	28						
3	Feb. 20	END	32	29	37	1037	0.35	1.30	428
		OCE	26						
4	Feb. 25	END	42	42	20	840	0.65	1.60	798
		OCE	42						
5	March 1	END	37	37	45	1665	0.70	1.20	685
		OCE	37						
6	March 5	END	27	27	34	918	0.40	1.60	308
		OCE	27						

Residence times are wind shift residence times, stress is maximum inertial-dissipation derived surface wind stress values, ratio is ratio of inertial-dissipation to bulk-estimated wind stress values, and total heat is maximum bulk-derived total heat flux, END, R/V *Endeavor*; OCE, R/V *Oceanus*.

*Uncertainty ±4 hours, determined subjectively by two persons for each ship.

†Uncertainty ±5 km h^{-1}, based on observed ranges of buoys (five) and ships (two, mostly).

‡Uncertainty ±25%, based on relative errors of storm residence times and speed, assuming independence.

§Uncertainty ±15%, based on relative error analysis.

believe it is a good approximation of the forcing translation speed, based on comparison of the front and wind maxima with ship data when their relative positions allowed it. Frontal translation speeds were estimated on the basis of ship and buoy vector wind and temperature time series, with guidance from the weather maps. Before the frontal passage at the ships or the buoys, certain wind speeds and directions prevailed. After passage these winds changed to different prevailing speeds and directions. The speed of the front was estimated by approximating the value of the wind speed component normal to the front, using the wind speed and direction immediately following the frontal passage. An initial attempt to use the time difference between passages at the ship and buoy locations and the location spacing was abandoned because the buoys were too close together and the ship locations were irregular with respect to the front orientation. The wind speed used for this estimate was generally not the maximum associated with individual storms because the maximum speed most often occurred in the cold air well behind the front. The storm (forcing) length scales were determined from the local residence times and the translation speed, assuming a frozen pattern and constant speed over the ship and buoy distance.

5.1. *February 13: Moderate Storm, Large Drop in Air Temperature, Gradual Recovery of Forcing Parameters*

This storm system was moderate in terms of wind speed for the Phase II period. The significance of this system was its effect, in combination with a system that followed, on the near-inertial ocean response (see Weller et al.). This storm system occurred shortly after the ships departed Bermuda, on February 12 and 13 for the R/V *Endeavor* and R/V *Oceanus*, respectively. The system was a major trough that moved off the east coast early on February 12. A cold front was analyzed by NMC and found to be approaching the FASINEX area near 1200 UT on February 13 (Figure 7*a*). A wind shift from westerly to northwesterly and a temperature drop near 0600 UT on February 13 were the only indications of the frontal passage. The main effects of the extensive eastward propagating system actually occurred with the passage of a secondary trough that first appeared on the NMC analysis at 1200 UT on February 13 (Figure 7*a*).

The approach of the secondary trough caused winds to shift clockwise from west to north and caused speeds to increase above 12 m s^{-1} at the R/V *Endeavor* and above 15 m s^{-1} at the R/V *Oceanus*. When the trough passed, the *Oceanus* had just arrived in the area and was located northeast of the *Endeavor* along a line nearly parallel to the NMC-analyzed trough. After the clockwise-rotating wind maxima passages, wind speeds decreased to levels just above 5 m s^{-1} for a 24-hour period and shifted from northeast to southwest. This reduction in wind forcing for an approximate near-inertial period is believed to have been important in the measured ocean response reported by Weller et al.

The speed of the trough, estimated on the basis of the NMC-analyzed positions and the buoy and R/V *Endeavor* time series, was approximately 27 km h^{-1}. The local residence time, estimated on the basis of the westerly to easterly wind shift interval and the wind maximum interval at the *Endeavor*, was 26 hours. The local residence time estimate approximates the inertial period of 25 hours for this location. The estimated trough speed and local residence time lead to a calculated spatial scale of 702 km, which is nearly the same as the 700-km estimate of Weller et al.

This storm also caused relatively large thermal forcing in the SST front region. Temperature decreases of 6° to 7°C behind the passage were exceeded only by the February 26 storm, and caused up to 8°C air-sea temperature differences. The large air-sea temperature and humidity differences occurring with the wind maximum near 13 m s^{-1} resulted in total heat flux values above 500 W m^{-2} for a period of 6–9 hours. Values above 600 W m^{-2} were calculated for a 1-hour period. The air-sea temperature difference and total heat flux decreased as the winds became easterly and then southerly, with the approach of another frontal system.

5.2. *February 15: Moderate Storm, Rapid Recovery of Forcing Parameters*

This system immediately preceded an between-storm period (February 16–18) described in detail by *Friehe et al.* [this issue]. The near-inertial response of the ocean to the sequential passages of these two moderate storms was the largest reported by Weller et al. for Phase II. In both storm periods the wind direction varied clockwise from southwesterly-westerly to northeasterly, and the maximum wind speeds were near 13 m s^{-1}. The peak values of clockwise-rotating wind stresses for this and the previous storm were separated by approximately 48 hours. The wind increase in this storm commenced approximately 24 hours after winds diminished from the previous storm.

On February 14 the synoptic-scale features were controlled by the intensification of the high-pressure cell after the frontal passage late on February 13 (Figure 7*a*). On February 15 a deepening 500-mbar trough and associated surface low-pressure system began to affect the area by 1000 UT, increasing the sea level pressure gradient that caused an increase in winds, from near 5 to above 15 m s^{-1}. A cold front associated with the northeastward moving low-pressure system passed both the R/V *Oceanus* and the R/V *Endeavor* shortly before 0000 UT on February 16. The approaching and passing front caused clockwise wind direction shifts and nearly 3°C drops in air temperature at both ships. The average speed of the cold front was again near 27 km h^{-1}, determined from ship and moored buoy time series data.

This storm would be classed as moderate within the range of storms being discussed. Wind stress measured on the R/V *Endeavor* increased to 0.50 N m^{-2}, which is more than 75% higher than drag coefficient predictions by the *Smith* [1988] formulation. A significant change for ocean forcing consideration was the rapid clockwise shift in wind direction, from southwesterly to northwesterly, associated with the cold front passage. The local residence time for the clockwise vector wind shift was estimated to be near 30 hours (Table 1) or slightly longer than the near-inertial period. The distance between the southwest and northeast winds, as calculated from the frontal speed and local residence time, was 810 km and again is in the range of the 700-km estimate of Weller et al., in view of the uncertainties in the estimates.

The sea-air temperature difference increase behind the front was moderate for this FASINEX set of storms, with a maximum of 5°C, but the effect was significantly diminished within 36 hours after frontal passage (see Figures 5 and 6). The maximum total heat flux with the maximum air-sea temperature difference was near 400 W m^{-2}, with a maximum of 479 W m^{-2} calculated for the R/V *Oceanus*. There was a very short period of winds parallel to/from the warm side of the SST front prior to the cold front passage. During this period the surface layer stratification became increasingly more neutral at the R/V *Oceanus* and more stable at the R/V *Endeavor* for a brief period.

After the cold front passage, surface wind stress and stratification at both ships returned quickly (within 6 hours) to low forcing values. In particular, the wind speeds decreased to values below 8 m s^{-1} within 4 hours and remained below 10 m s^{-1} for the rest of the day as the subtropical high redeveloped. The low forcing after the moderate forcing of these two sequential storms probably was an important factor in the observation of very large near-inertial ocean responses by Weller et al.

5.3. *February 20: Sharp Air Temperature Drop, Prolonged Surface Stress Enhancement*

Early on February 20 a weak high-pressure system dominated the area, but sea-level pressure fell throughout the day as a developing wave associated with a front moved off the coast and through the FASINEX area (Figure 7*c*). Winds were southerly at 5–8 m s^{-1} early in the day, but shifted clockwise to westerly, then to northwesterly at 10–12 m s^{-1} as the cold front passed the ships (at 1430 UT for the R/V *Endeavor*, 1800 UT for the R/V *Oceanus*). Similar maximum stress values near 0.40 N m^{-2} were observed at the *Oceanus* and *Endeavor* just prior to the cold front passages. The frontal speed was estimated, from buoy and ship time series data, to be 37 km h^{-1} or about 30% faster than the preceding frontal speed. The local residence time for the wind direction shift was estimated, on the basis of the two ship values, to be 29 hours, which was definitely larger than the near-inertial period even in view of the uncertainties in these estimates. A not too large extrema in the near-inertial amplitude, which peaked on February 24, began to occur on February 22 according to Weller et al. The distance between southerly and northerly winds was estimated from these values to be larger than 1073 km, or approximately 53% larger than the scale estimated by Weller et al.

The most dramatic drop in air temperature of all seven cold fronts was associated with this storm system. The R/V *Endeavor* experienced a 6°C and the R/V *Oceanus* a nearly 4°C decrease in air temperature as the cold front passed. This drop was not associated with a large cold air mass following the front, but by a convective band, described below, that accompanied this fast-moving front. The temperature drop was not just a mesoscale outflow from a local thunderstorm, because it was observed at both ships and it took 6 hours for the temperature to recover at the R/V *Endeavor*. The 6-hour (short duration) cold air burst apparently caused large heat fluxes at the R/V *Endeavor* that influenced across-front microstructure data described by Weller et al.

The time series of total heat flux from the ships (Figures 5*d* and 6*d*) also exhibit sharp peaks, above 400 W m^{-2} for a 3-hour period. These peaks are followed within 6 hours by maxima in the wind stress values (Figures 5*e* and 6*e*). The combination of these factors could have been a primary reason for the high values in the ratio of upper layer turbulent kinetic energy to the total kinetic energy at a 10-m depth. Weller et al. found the ratio to be 5–10 times higher than observed in other open-ocean regions.

The intensity of the front was also evident in hourly GOES images that showed the convection line move across the FASINEX region in a southeasterly direction, leaving the north end of the FASINEX area mostly clear. Photographs taken from the NOAA P-3 on the approach to the area from the west at around 1500 UT showed a deep multilevel cloud structure over the area. Scattered clouds were present at the ships in the early part of the day, but increased, becoming broken with rain occurring at 0700 UT. A severe thunderstorm was experienced at the R/V *Oceanus* from 1735 to 1740 UT.

It was fortunate that aircraft data was collected in the vicinity of the cold front, providing a three-dimensional description of this strong system. The character of the storm system determined by the aircraft flight matched that recorded at the ships. The NOAA P-3 arrived at the northern end of the FASINEX measurement region at 1530 UT on February 20. At this time the region was under deep clouds and rain. The aircraft flew south at 150-m altitude from a position of 29.1°N, 70.2°W to a position of 27.4°N, 69.7°W. In the convection region at the northern end of this leg, the winds were variable in speed and direction. At 28.5°N, 70.0°W (1548 UT) the aircraft flew ahead of the atmospheric front. Air temperature increased from 15° to 21°C, and wind speed increased to a steady 14 m s^{-1} from the southwest. This transition occurred just north of a 2°C sea-surface temperature discontinuity measured at 28.3°N, 69.9°W.

The aircraft performed a series of E–W tracks in a region of shallow cumulus under altostratus, at a latitude of 27.3°N. A well-defined inversion was measured at 1200 m. The 50-m fluxes measured by the aircraft were 230 W m^{-2} for latent heat and, within measurement error, zero for sensible heat flux. The stress magnitude was 0.19 N m^{-2}. The air-sea temperature difference was near zero at this time.

At 1730 the NOAA P-3 headed north at 150 m, passing through heavy rain and crossing the atmospheric front, which had moved south, at 28.0°N, 70.0°W (1745 UT). In crossing the front, air temperature dropped from 22° to 16°C and pressure dropped about 5 mbar. Winds strengthened to 18 m s^{-1}, and shifted to westerly. Conditions recovered rapidly behind the front, returning nearly to prefrontal levels of these variables. To the north, skies were mostly clear, air temperature was around 20°C, and pressure had increased 6 mbar from the low value at the front. The winds were stronger, around 14 m s^{-1}, and more steady, from the southwest, compared to measurements at the same location 2 hours earlier.

Aircraft maneuvers at 28°N found latent and sensible heat fluxes at 50 m to be quite low, 78 W m^{-2} and 5 W m^{-2}, respectively. The low latent heat flux was attributable to higher humidity in the air; the dew point depression behind the front was near zero.

This storm also affected the local air-sea interaction differently than the previous ones; the air-sea temperature difference was modified dramatically for a relatively short period of time, but the stress was increased for an extended period. Wind speeds for 24 hours after frontal passage were greater than prefrontal values, resulting in elevated surface layer wind stress values for an extended period. Air temperature, however, returned to the prefrontal value within 3 hours, then dropped gradually to a new level during approximately the next 12 hours, where it remained within a 2°–3°C range for at least 2 days (see Figures 5 and 6).

5.4. *February 25: Double Frontal Passage, Large Stress and Air-Sea Temperature Differences*

On February 25 a developing cyclone and an associated cold front located just east of Florida traveled on a northeasterly track and continued to deepen. From 0000–0600 UT the movement of the cold front toward the ships was quite slow, and by 0600 UT a secondary front had formed behind the first. The low-pressure frontal system took a more easterly track, bringing the fronts through the measurement region. It took approximately 9 hours for both distinct cold fronts to pass both ships. The first front was slower moving than previous ones and of moderate intensity, with approximately 2°C air temperature drops at the R/V *Oceanus* and R/V *Endeavor*. The second, secondary, front had an even lower estimated translation speed and air temperature drops of less than 1°C occurred at the ships.

The first front was not detectable at the buoy array, so its 20 km h^{-1} speed was estimated on the basis of ship time series only. The second front was detected at the buoy array, and its average speed of 8.5 km h^{-1} made it the slowest-moving front of the intensive measurement period detected by the buoys. When the first front passed the ships, R/V *Endeavor* at 1330 UT and R/V *Oceanus* at 1530 UT, wind speeds increased to 12 m s^{-1} prior to passage, but the winds remained southwesterly. When the second front passed the ships, R/V *Oceanus* at 2100 UT and R/V *Endeavor* at 2200 UT, wind speeds remained slightly below 10 m s^{-1}, and the winds shifted from westerly to northwesterly.

Weller et al. results show a near-inertial response to this frontal system, beginning after the storm passed on February 26, which reached a maximum just before the passage of a wind maximum of 20 m s^{-1} on March 1. The near-inertial amplitude maximum was 30% less than occurred after the faster-moving, but less intense, February 13 and 15 storms. The estimated local residence time was 42 hours, which, even with uncertainties of the estimate, is considerably longer than the near-inertial period.

In terms of mesoscale air-sea dynamics, this system was important for having next to the highest surface stress and the largest air-sea temperature differences observed during the Phase II intensive measurement period. The maximum forcing in the February 25–27 period occurred in the cold air behind the second front, nearly 18 hours after its passage. Both ships measured peak stress values near 0.65 N m^{-2}, which were 60% higher than the bulk estimated values, and differences in sea and air temperature were larger than 6°C. A maximum total heat flux value of 798 W m^{-2} was calculated for the R/V *Oceanus* and values above 600 W m^{-2} occurred for more than 6 hours. This period had the largest calculated total heat flux of the intensive data collection period.

Air-sea interaction forcing effects of this storm system were prolonged, since it was a slow-moving system, complicated with a secondary front. The translation speed, based on the speed of the first front, was the lowest estimated for Phase II, at approximately 20 km h^{-1}. The air temperature did not approach the temperature of the sea surface until nearly 60 hours after the passage of the second cold front. The surface stress did return to values more typical of a high-pressure situation within 24 hours.

5.5. *March 1: Highest Wind Speed Event*

The highest wind speeds experienced in Phase II (peak of 20 m s^{-1}, measured at the *Oceanus*) were associated with a cyclonic system that approached the area on March 1, with frontal passage at the ships just before 0000 UT on March 2. It was a rapidly developing cyclone, since it was analyzed at 0600 UT on March 1 as a weak (1008 mbar) open wave located roughly 600 km W–NW of the ships. It remained essentially stationary for the next 6 hours, deepening to 1005 mbar, then began to move northeastward. By 1800 UT on March 1 the central pressure had dropped to 996 mbar, and the cyclone's center was located approximately 450 km northwest of the ships (Figure 7*e*). In addition to having the largest stress values, near 0.8 N m^{-2} at the R/V *Endeavor*, this was the fastest moving system of Phase II when it passed the buoys, with an average speed of 45 km h^{-1}.

The observed near-inertial response to this storm began on March 2, according to Weller et al., and an amplitude maximum occurred on March 6. This maximum was exceeded only by that occurring in response to the sequential storms of February 13 and 15. The residence time of the clockwise wind shift from southerly to northerly was estimated to be 37 hours, or 50% longer than the near-inertial period. The long local residence time occurred because the size and track of the storm caused westerly winds for an extended period behind the front, not shifting to northwesterly until 24 hours after frontal passage at the R/V *Oceanus*; 15 hours for the R/V *Endeavor*. The estimated distance between southerly and northerly winds for this storm is greater than 1650 km, or more than 2 times the scale value estimated by Weller et al. to be representative for the region during the FASINEX period.

Wind speed, air temperature, surface stress, and stratification all changed gradually behind the front, taking many hours to level off: 72 hours in the case of air temperature, 24 hours for the wind speeds. The cold air behind the front caused sea-air temperature differences up to 4.5°C at R/V *Endeavor*, 3°C at R/V *Oceanus*. The maximum total heat flux occurred with the wind maximum, rather than the air-sea temperature difference maximum. The maximum was 685 W m^{-2}, and values near 600 W m^{-2} were maintained for almost 6 hours.

The importance of the SST front on a local scale, even with a storm of this intensity, can be seen in the R/V *Oceanus* temperature trace on March 3. As the *Oceanus* crossed the SST front, the air temperature responded, following the same pattern. This illustrates that interactions and forcing occur simultaneously on different scales after the passage of a storm.

5.6. *March 5: Noticeable Small-Scale SST Frontal Effects Concurrent With a Maximum in Near-Inertial Amplitudes*

The front that transited the FASINEX area on March 5 was associated with a complex surface low-pressure system that stalled west of the area for a day, then moved rapidly through the region (Figure 7*f*). A weak wave developed along this front, causing the southward extending trough and associated front to intensify before transiting the FASINEX area.

The cold front passed the ships around 2100 UT on March 5, and both experienced rapid clockwise wind shifts, from S–SW to NW, and speed maxima slightly less than 15 m s^{-1}, shortly after the passages. These forcing events occurred approximately 90 hours after the maximum winds with the previous storm, near 0000 UT on March 2. It is evident from wind and temperature changes in Figures 5 and 6 that this system was not as intense as the systems on either March 1–2 or February 25–26. A maximum stress value of 0.35 N m^{-2} was observed at the R/V *Oceanus*, which is 50% less than the maximum value observed at R/V *Endeavor* with the March 1–2 storm. The air temperature decrease behind the front was 2°C, compared with 5°–6°C decreases on February 25 and March 1–2. Extrema in total heat fluxes were only near 300 W m^{-2}. Wind speeds with this storm decreased to below 5 m s^{-1} within 15 hours after the maxima.

Observed near-inertial amplitude extrema at the moorings (see Weller et al.), began on March 3 and reached maxima near 0000 UT on March 6. The near-inertial maximum amplitude at one mooring was only exceeded during Phase II by maxima following the passages of the February 13 and 15 storms.

A clear example of the SST front influencing mesoscale variations of air-sea interaction occurred with this moderate large-scale atmospheric forcing event. Advection of warm air in the warm sector of this system caused slightly stable stratification conditions at the R/V *Oceanus* and near-neutral conditions at R/V *Endeavor* during wind speed maxima (Figures 5*d* and 6*d*). Since SST values measured at both ships were higher than those on the cold side of the SST front, horizontal variations of surface layer stratification, which is important to wind forcing, can be assumed to have existed across the SST front for at least 6 hours prior to frontal passage. Similar horizontal variations in stratification probably occurred with moderate southerly flow across the SST front during February 18–19, as described by *Friehe et al.* [this issue] on February 24, which was prior to the passage of the February 25–26 storm and just prior to the frontal passage on March 1.

6. OCEAN SURFACE EFFECTS ON REGIONAL MABL VARIABILITY

The presence of sea surface temperature fronts gives rise to atmospheric effects that do not occur in oceanic areas of small surface temperature gradients. FASINEX therefore provided an opportunity to study the mesoscale variations in the atmosphere brought on by an SST front. One can see this influence most clearly in the absence of atmospheric storm systems. Certain characteristics were commonly found in the mesoscale structure of the atmospheric boundary layer, which were modified by oceanic forcing. Typical boundary layer properties will be presented first, followed by a discussion of variations caused by discontinuities in the sea surface temperature field.

6.1. *Mean MABL Structure in Vicinity of SST Front*

During undisturbed periods the marine atmospheric boundary layer was characterized by the existence of a layer well mixed in potential temperature and specific humidity. Above this mixed layer was a transition layer that was topped by an inversion. Examples of this structure can be seen in Figure 8, which presents radiosonde profiles from R/V *Endeavor*. Multiple inversions were common. Possible causes of these multiple layers are discussed by *Rogers*

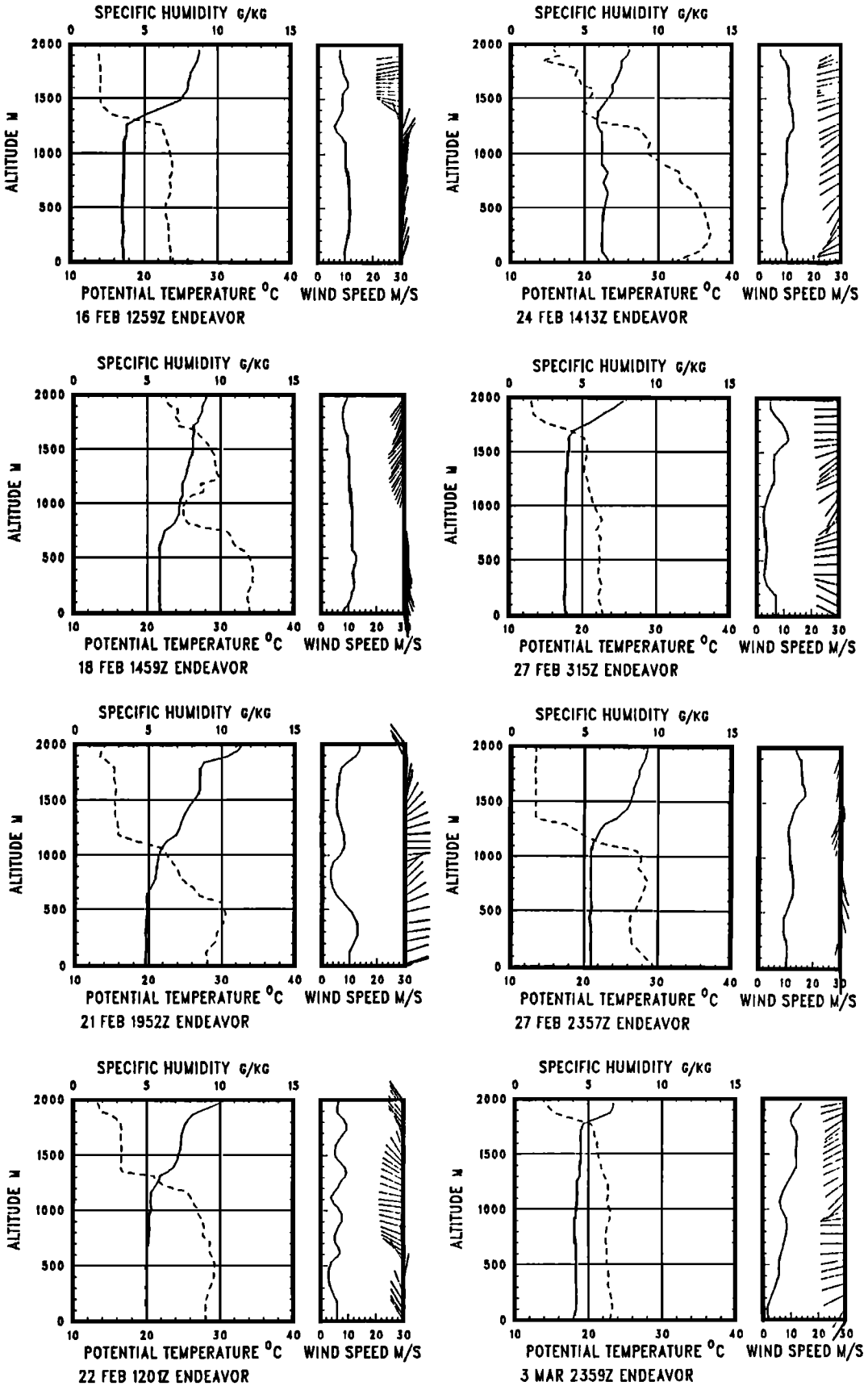

Fig. 8. Rawinsonde-derived profiles of potential temperature (in degrees Celsius), indicated by solid curves, and specific humidity (in grams per kilogram) indicated by dashed curves from the R/V *Endeavor* for indicated times.

[1989]. The dominant cloud types in these "undisturbed" periods in between storm systems were low-level to midlevel stratus and stratocumulus as well as fair-weather cumulus. Precipitation did not usually occur under these circumstances. The general pattern of well-mixed, transition and inversion layers was representative, but there was a wide range in inversion heights and absolute values of potential temperature and mixing ratio in the mixed layer. Figure 8 gives a general idea of the range of mixed layers that developed during Phase II. *Fellbaum et al.* [1988] present a complete set of radiosonde profiles from the R/V *Endeavor* and R/V *Oceanus* and a daily description of the weather conditions experienced at the ships.

6.2. *SST Frontally Induced MABL Phenomena*

Several mesoscale features of the MABL in the vicinity of the SST front can be attributed mainly to oceanic forcing. Secondary atmospheric circulations, the formation of an internal boundary layer (IBL) within the MABL, and maintenance of elevated mixed layers are all related to the SST gradient. Wind direction, air-sea temperature differences, and the state of atmospheric equilibrium with the ocean surface all play a part in determining the MABL structure, but the main factor in these particular features is the discontinuity in sea surface temperature.

Evidence for SST frontally induced secondary atmospheric circulations has been presented by *Khalsa and Greenhut* [1989]. They showed entrainment rates to be larger on the warm side of the SST front. However, the wind direction is an important consideration, as discussed by *Friehe et al.* [this issue]. On the day Khalsa and Greenhut investigated, February 17, the wind was easterly, parallel to the SST front. *Friehe et al.* [this issue] studied this case in connection with February 16 and 18, when the wind was blowing across the SST front, first from the north, and on February 18 from the south.

Model results and FASINEX data agree on the formation of an internal boundary layer within the MABL when warm air flows from relatively warm to relatively cold water. The IBL is different in structure from the rest of the MABL. *Rogers et al.* [1990] provide further analysis of February 18, including data from the NCAR Electra. *Rogers* [1989] discussed the vertical structure of the MABL in the vicinity of the SST front, including the IBL and the presence of multiple cloud-capped mixed layers.

The interaction of the atmospheric forcing and oceanic forcing determines the existence of these MABL features. Figures 5*b* and 6*b* provide a summary of periods when the wind was roughly parallel to the SST front (from the east or west), and when it blew across the front (from the north or south).

6.3. *SST Front Influence on Vertical MABL Variability*

Radiosonde profiles can be used to determine what, if any, effect the SST front had on the height of MABL features such as mixing height and dry layers. Profiles taken on opposite sides of the SST front may appear similar, but prominent features may occur at higher elevations on one side of the front than on the other. *Hsu et al.* [1985] presented data supporting the theory that in the absence of significant advective forces, the top of the mixed layer should be higher on the warm side of the SST front than on the cold side. FASINEX provided very few cases which met all the criteria required to verify the results of Hsu et al., but there are a number of sounding pairs from opposite sides of the SST front that can be informative in understanding differences in MABL structure across the front.

Figure 9 presents profiles of some of these sounding pairs; Table 2 provides information on meteorological conditions at launch time as measured at the ships. As Table 2 indicates, all pairs include one sounding from the R/V *Endeavor* and one from the R/V *Oceanus*, taken on opposite sides of the SST front, within 1 hour of each other. A value of 22.5°C was used for this analysis to mark the SST front. The sounding pairs shown in Figure 9 were taken during the period February 16–18. This period was examined, as stated earlier, by *Friehe et al.* [this issue]. The importance of the wind direction in connection with the presence of the SST front can be seen in Figure 9. On February 18, when the wind was from the south, blowing across warm water toward cold water (Figure 9) the MABL is seen to be deeper, as well as drier and warmer, on the warm side of the SST front, at the R/V *Oceanus*. However, in Figure 9, from very late on February 16 through very early February 18, when the wind was from the east, and E–SE, there is no deepening of the MABL on the warm side of the SST front (at the R/V *Oceanus*).

7. CONCLUSIONS

One purpose of this paper was to determine whether the atmospheric conditions encountered during FASINEX were representative of the region. The general applicability of FASINEX studies depends, in part, on how this period compares with climatology. The intensive measurement period, from January through March, has been shown to compare favorably with climatology. In terms of air-sea temperature differences, surface pressure and temperature patterns, cloud cover, and storm tracks and frequency, the conditions can be considered typical for this time of year.

Little connection was found between the SST front and regional cloudiness, either on a daily or monthly scale. The cloud field was shown to vary considerably on a daily time scale, as can be inferred from the surface solar irradiance variability. Cloudiness was found to increase smoothly from south to north, suggesting a minimal effect of the thermal front on the mean cloudiness.

Characteristics of storm systems, such as the air temperature behind the cold front, wind speed, and speed of the system itself, were important in determining the magnitude of atmospheric forcing parameters. Air-sea temperature differences and surface wind stress were seen to remain elevated for up to 72 hours after the passage of a cold front. The extended influence of storm systems through surface fluxes must be considered in dynamics studies. The forcing due to storms may reach a peak quite rapidly in association with a cold front passage, but can die off rather slowly over a period of 1–3 days.

Observed ocean responses [*Weller et al.*, this issue] could be more readily related to cyclones and associated front tracks through the FASINEX region and their residence times than to the magnitude of the wind forcing. The clockwise rotation of the wind during maximum forcing and the duration (residence times) of the forcing periods was shown to be as important to observed near-inertial responses

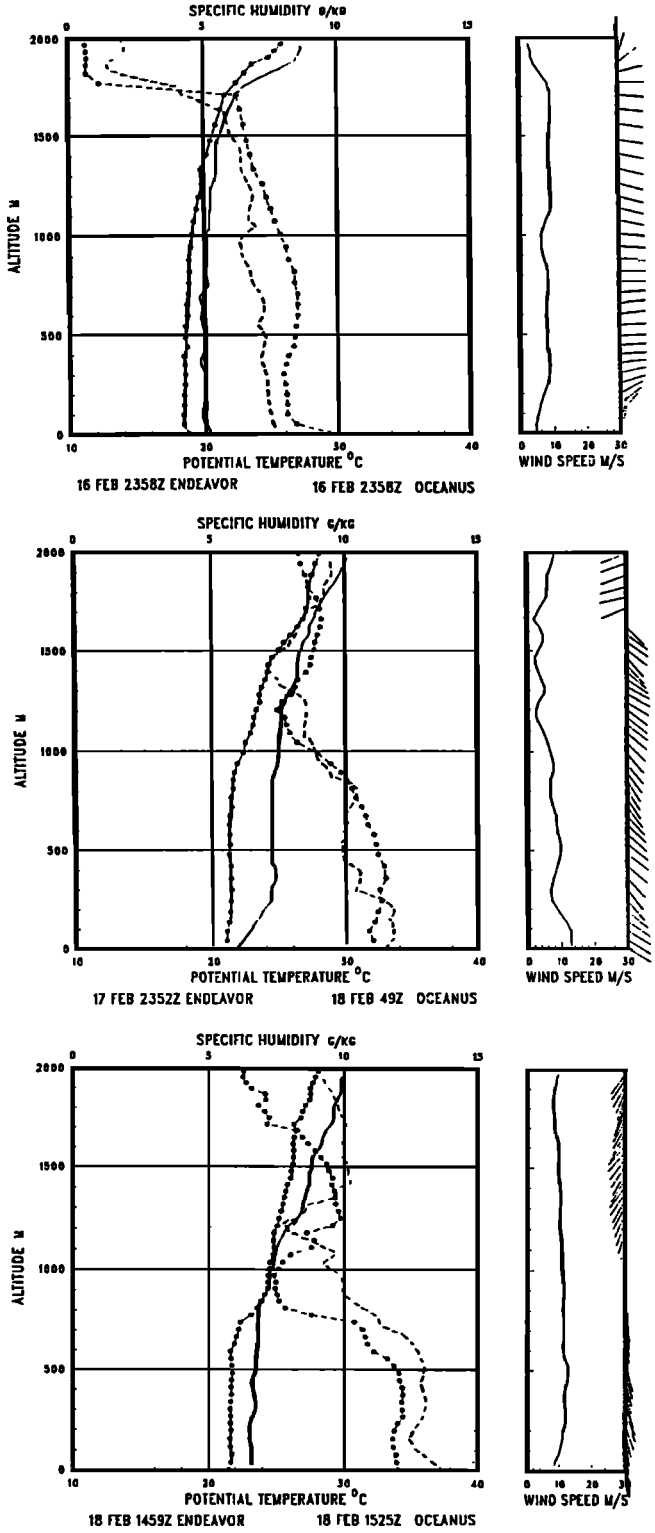

Fig. 9. Rawinsonde-derived profiles of potential temperature (in degrees Celsius), indicated by solid curves, and specific humidity (in grams per kilogram), indicated by dashed curves, taken on opposite sides of the SST front. Dotted lines show R/V *Endeavor*; plain lines, R/V *Oceanus*. Wind profiles (in meters per second) are from R/V *Endeavor*.

in the ocean as the magnitude of the wind maxima. The clearest example of this is a comparison of the large ocean response to the sequential passage of two moderate storms over the February 13–16 period, with the lower response to the storm passage on March 2, which had 35% larger wind stress values and a 30% longer period of maximum forcing.

These results show that the effect of local ocean surface variations cannot be neglected even in the presence of large-scale atmospheric forcing, as the storm of March 1 has shown. The ships' records indicated that the air-sea temperature difference, and hence the heat flux, varied noticeably across the SST front after the cold front had passed.

TABLE 2. FASINEX Sounding Pairs

System	Date	Ship	Time, UT	SST, °C
1	Feb. 16	OCE	2358	23.36
	Feb. 16	END	2358	21.01
2	Feb. 17	END	2352	21.86
	Feb. 18	OCE	0049	23.33
3	Feb. 18	END	1459	21.30
	Feb. 18	OCE	1525	23.32

Soundings were taken when ships were on opposite sides of the SST front, and were within approximately 2 hours of each other. OCE, R/V *Oceanus*; END, R/V *Endeavor*.

REFERENCES

Barston, A. A., The global climate for March–May 1986: Continued uncertainty about the possible onset of an ENSO episode, *Mon. Weather Rev.*, *115*, 317–335, 1987.

Bates, J., and C. Gautier, Interaction between net surface shortwave flux and sea surface temperature, *J. Appl. Meteorol.*, *28*(1), 43–51, 1989.

Betts, A. K., and B. A. Albrecht, Conserved variable analysis of the convective boundary layer thermodynamic structure over the tropical oceans, *J. Atmos. Sci.*, *44*, 83–99, 1987.

Eriksen, C. C., R. A. Weller, D. L. Rednick, R. T. Pollard, and L. A. Regier, Ocean frontal variability in the Frontal Air-Sea Interaction Experiment, *J. Geophys. Res.*, this issue.

Fairall, C. W., J. B. Edson, S. E. Larson, and P. G. Mestayer, Inertial-dissipation air-sea flux measurements: A prototype system using real-time spectral computations, *J. Ocean Atmos. Technol.*, *7*, 425–453, 1990.

Fellbaum, S. R., S. H. Borrmann, P. A. Boyle, K. L. Davidson, W. G. Large, T. Neta, and C. A. Vaucher, Frontal Air-sea Interaction Experiment (FASINEX) shipboard meteorology data and weather atlas, *NPS-63-88-002*, Nav. Postgrad. Sch., Monterey, Calif., 1988.

Friehe, C. A., W. J. Shaw, D. P. Rogers, K. L. Davidson, W. G. Large, S. A. Stage, G. H. Crescenti, S. J. S. Khalsa, G. K. Greenhut, and F. Li, Air-sea fluxes and surface-layer turbulence around a sea surface temperature front, *J. Geophys. Res.*, this issue.

Hanson, H. P., P. Cornillon, G. R. Halliwell, Jr., and V. Halliwell, Climatological perspectives, oceanographic and meteorological, on variability in the subtropical convergence zone in the northwestern Atlantic, *J. Geophys. Res.*, this issue.

Hsu, S. A., R. Fett, and P. E. La Violette, Variations in atmospheric mixing height across oceanic thermal fronts, *J. Geophys. Res.*, *90*, 3211–3224, 1985.

Khalsa, S. J. S., and G. K. Greenhut, Atmospheric turbulence structure in the vicinity of an oceanic front, *J. Geophys. Res.*, *94*, 4913–4922, 1989.

Large, W. G., and S. Pond, Open ocean momentum flux measurements in moderate to strong winds, *J. Phys. Oceanogr.*, *11* 324–3336, 1981.

Rogers, D. P., The marine boundary layer in the vicinity of an ocean front, *J. Atmos. Sci.*, *46*, 2044–2062, 1989.

Rogers, D. P., C. A. Friehe, and W. J. Shaw, Surface layer turbulence over a sea surface temperature front, paper presented at 9th Symposium on Turbulence and Diffusion, Am. Meteorol. Soc., Roskilde, Denmark, April 29–May 3, 1990.

Skupniewicz, C. E., and K. L. Davidson, Hot-film measurements from small buoy: Surface wind stress estimates using the inertial dissipation method, *J. Ocean Atmos. Technol.*, in press, 1991.

Smith, S. D., Coefficients for sea surface wind stress, heat flux, and wind profiles as a function of wind speed and temperature, *J. Geophys. Res.*, *93*, 15,467–15,472, 1988.

Weller, R. A., An overview of the Frontal Air-Sea Interaction Experiment (FASINEX): A Study of Air-Sea Interaction in a region of strong oceanic gradients, *J. Geophys. Res.*, this issue.

Weller, R. A., D. L. Rudnick, C. C. Eriksen, K. L. Polzin, N. S. Oakey, J. W. Toole, R. M. Schmitt, and R. T. Pollard, Forced ocean response during the Frontal Air-Sea Interaction Experiment, *J. Geophys. Res.*, this issue.

Whittaker, L. M., and L. H. Horn, *Atlas of Northern Hemisphere Extratropical Cyclone Activity, 1958–1977*, Department of Meteorology, University of Wisconsin, Madison, 1982.

Woodruff, S. D., R. J. Slutz, R. L. Jenne, and P. M. Stwurer, A comprehensive ocean-atmosphere data set, *Bull. Am. Meteorol. Soc.*, *68*, 1239–1250, 1987.

P. J. Boyle, Department of Meteorology, MR/Bp, Naval Postgraduate School, Monterey, CA 93943.

K. L. Davidson, Department of Meteorology, MR/Ds, Naval Postgraduate School, Monterey, CA 93943.

C. Gautier, Department of Geography, University of California at Santa Barbara, Santa Barbara, CA 93106.

H. P. Hanson and S. J. S. Khalsa, Cooperative Institute for Research in Environmental Sciences, P. O. Box 449, Boulder, CO 80309.

(Received December 6, 1990;
revised February 13, 1991;
accepted February 13, 1991.)